


Multiple charge density waves compete in ternary rare-earth nickel carbides, $RNiC_2$ (R : Y, Dy, Ho, and Er)

Hiroyuki Maeda, Ryusuke Kondo ^{*}, and Yoshio Nogami
Department of Physics, Okayama University, Okayama 700-8530, Japan

 (Received 7 May 2019; revised manuscript received 19 August 2019; published 9 September 2019)

Single-crystal x-ray-diffraction experiments and electrical resistivity measurements were performed on intermetallic compounds of formula $RNiC_2$ [rare earth (R): Y, Dy, Ho, and Er]. In the series of diffraction studies, we found three kinds of satellite reflections that had different wave vectors [incommensurate $\mathbf{q}_{1ic}:(0.5, 0.5 + \eta, 0)$ and commensurate $\mathbf{q}_{1c}:(0.5, 0.5, 0)$ and $\mathbf{q}_{2c}:(0.5, 0.5, 0.5)$] at temperatures where their resistivities show anomalies, such as a hump, a sharp increase, or a dent. Satellite reflections with nearly identical wave vectors have also been reported in $RNiC_2$ composed of earlier lanthanide atoms ($GdNiC_2$ and $TbNiC_2$). These results indicate the formation of a charge density wave (CDW) also in $RNiC_2$ studied in this paper. We found strong competition between the \mathbf{q}_{1ic} and the \mathbf{q}_{2c} CDWs in $DyNiC_2$ and $YNiC_2$, and that only the \mathbf{q}_{2c} CDW existed in $HoNiC_2$ and $ErNiC_2$. Based on the results obtained in the present paper and those of $SmNiC_2$, $GdNiC_2$, and $TbNiC_2$ reported before, we discuss the CDW transitions in the $RNiC_2$ family.

DOI: [10.1103/PhysRevB.100.104107](https://doi.org/10.1103/PhysRevB.100.104107)

I. INTRODUCTION

Since the synthesis of ternary rare-earth nickel carbides $RNiC_2$ [rare earth (R)] [1], their various magnetic properties had been intensively studied. These compounds possess a $CeNiC_2$ -type crystal structure with an orthorhombic lattice and $Amm2$ space group without inversion symmetry. Since $LaNiC_2$ and $YNiC_2$ show conventional Pauli paramagnetism [2], the nickel atom and nonmagnetic carbon atoms are supposed to have no contribution to the magnetic properties of $RNiC_2$. Thus, only the rare-earth atoms contribute to its magnetic properties, and various magnetic orders are exhibited at low temperatures based on their Ruderman-Kittel-Kasuya-Yosida (RKKY) interactions. Except for $SmNiC_2$, which shows ferromagnetic properties, and $PrNiC_2$, which has no magnetic order down to 1.5 K [3], $RNiC_2$ are antiferromagnets with characteristic magnetic orders and phenomena, such as simple collinear commensurate order (R : Nd, Er, and Tm) [4–6], noncollinear commensurate order (R : Gd and Tb) [7–11] and commensurate order with an incommensurate-commensurate (IC-C) transition (R : Ce, Dy, and Ho) [6,12–15].

Subsequently, a charge density wave (CDW) transition and remarkable interplay between the CDW and its ferromagnetic order on the constituent rare-earth atoms were discovered in one member of the $RNiC_2$ family $SmNiC_2$ [16,17]. A CDW transition is one representative phenomenon that can be realized in low-dimensional electronic systems [18], and the quasi-one-dimensional (1D) electronic nature of $RNiC_2$ was soon confirmed using first-principles calculations [19]. In $SmNiC_2$, an incommensurate CDW (IC CDW) with the reduced wave vector $(0.5, 0.5 + \eta, 0)$, which forms at

148 K, is completely destroyed at the ferromagnetic order temperature 18 K. After this discovery, various other experimental results involving CDWs in $RNiC_2$ have been reported [20], such as the crystal structure of $SmNiC_2$ with the IC CDW [21], interplay between CDWs and antiferromagnetic orders [22–25], and interplay between the IC CDW and a ferromagnetic order induced by an external magnetic field [26,27]. Thus, the $RNiC_2$ family, which has various magnetic orders at low temperatures, has become the standard material for investigating the interplay between CDW and magnetic order. Despite the unclear understanding of the interplay mechanism in the $RNiC_2$ family materials, the reason why these materials are the standard for studying relationships between CDW and magnetic order is that such clear interplay phenomena have yet to be observed in any other materials thus far [28–30].

As the studies of materials in the $RNiC_2$ family have developed, various phenomena concerning CDWs have been discovered. For example, another long-range CDW was discovered in $RNiC_2$ formed from the middle lanthanides. This commensurate CDW (C CDW), the reduced wave vector of which is $(0.5, 0.5, 0.5)$, was first recognized in $SmNiC_2$ as diffuse spots without long-range order [16], and then it appears in $TbNiC_2$ as sharp reflections with long-range order [31]. An IC-C transition from $(0.5, 0.5 + \eta, 0)$ to $(0.5, 0.5, 0)$ was also discovered in $GdNiC_2$ and $TbNiC_2$ [31]. Based on these structural studies and transport measurements, CDW phase diagrams of the $RNiC_2$ family were proposed by Shimomura *et al.* [31] and Roman *et al.* [32] and Kolincio [33], respectively. However, their phase diagrams were a little incomplete because the former diagram was only for $RNiC_2$ (R : La–Tb), and only two out of the above three CDWs, IC CDW and C CDW resulted from the IC-C transition, were considered in the latter one.

In this article, we present the electrical and structural properties of nonmagnetic $YNiC_2$ and the antiferromagnets,

^{*}kondo@science.okayama-u.ac.jp

DyNiC₂, HoNiC₂, and ErNiC₂ as obtained from single-crystal samples. These compounds were synthesized because we considered that according to the proposed phase diagram by Shimomura *et al.* [31], these two CDWs, IC CDW [the wave vector of which is about $(0.5, 0.5 + \eta, 0)$] and C CDW [the wave vector of which is $(0.5, 0.5, 0.5)$], seemed to appear at almost the same temperatures and were expected to compete strongly when R : Dy–Er. We have found strong competition between the IC CDW and the C CDW in YNiC₂ and DyNiC₂ in a narrow temperature range, and that only the C CDW exists in HoNiC₂ and ErNiC₂. Furthermore, we discuss the CDW transitions of RNiC₂ with the middle lanthanides (R : Y, Sm, Gd, Tb, Dy, Ho, and Er). We also discuss the interplay between CDWs and magnetism in antiferromagnetic compounds (DyNiC₂, HoNiC₂, and ErNiC₂) based on the temperature dependence of the resistivity and the CDW satellite reflection intensities below and above their magnetic transition temperatures.

II. EXPERIMENTAL PROCEDURE

All compounds were synthesized using the conventional argon-arc technique. The purities of the ingredients were 99.9% pure for Y, Dy, Ho, and Er, and 99.99% pure for Ni and C. In the arc-melting process, each ingot was melted and turned over several times to improve homogeneity. As a result of this process, many small platelike crystals were found on the surface of each ingot. These crystals were removed for further analysis.

Before every electrical and structural measurement, the samples were verified by lattice constant measurements using a conventional four-circle x-ray diffractometer for single-crystal structure analysis, AFC7R (Rigaku Co.) with Mo $K\alpha$ radiation. This measurement revealed that most of the as-grown crystals on the surface of an ingot had a twin structure: The a axis is completely parallel in a crystal, but the b - c plane stacks in two diagonal lines ($b + c$ and $b - c$). A typical crystal size was $0.3 \times 0.7(\parallel b + c \text{ or } b - c) \times 0.2(\parallel a) \text{ mm}^3$. In the case of poor sample quality, the samples were wrapped in tantalum foil, sealed in an evacuated quartz tube, and annealed at 1100 °C for a week to improve sample quality.

Electrical resistivity was measured using the conventional four-probe method along the longest direction ($\parallel b + c$ or $b - c$). Temperature dependences of the resistance of each sample were measured using a commercial physical property measurement system, (Quantum Design) from room temperature to 2 K.

X-ray satellite reflections were studied in the following procedures: First, rough positions of satellite reflections were investigated by the photographic method using imaging plate (IP), and next, their precise positions were determined employing a unique four-axis design x-ray diffractometer equipped with a scintillation detector [34].

In the case of YNiC₂, HoNiC₂, and ErNiC₂, which have resistance anomalies above 100 K, a commercial x-ray-diffraction measurement system with a large-area curved IP and Cu $K\alpha$ radiation from a rotating anode source with a confocal multilayer x-ray mirror, R-AXIS RAPIDII (Rigaku Co.), was employed. This system was equipped with a gas-blowing-type temperature controller (measurement range =

400–90 K). The typical voltage and current of the x-ray generator were 40 kV and 30 mA, respectively. In the case of DyNiC₂, which shows a resistance anomaly below 100 K, the so-called fixed-sample fixed-film *monochromatic Laue method* was employed using Mo $K\alpha$ radiation monochromatized and focused by a singly bent graphite, generated from a rotating anode source. This system was equipped with a Gifford-McMahon refrigerator, and its measurement range was from 300 to 10 K. To avoid generating a $\lambda/2$ component, the typical voltage and current of the x-ray generator were 34 kV and 135 mA, respectively.

For the determination of precise wave vectors of observed satellite reflections, a unique four-axis design x-ray diffractometer with monochromatized Mo $K\alpha$ radiation from an x-ray tube and a scintillation detector was employed [34]. This diffractometer was also used for collecting the intensity variations of CDW satellite reflections between above and below the magnetic ordering temperature, down to 4 K. To avoid generating a $\lambda/2$ component, the typical voltage and current of the x-ray generator were 34 kV and 30 mA, respectively.

III. EXPERIMENTAL RESULTS

Table I shows the lattice parameters and magnetic properties of the target compounds: YNiC₂, DyNiC₂, HoNiC₂, and ErNiC₂. Those of SmNiC₂, GdNiC₂, and TbNiC₂ are also listed for discussion [16,31]. Our discussion will start with the nonmagnetic compound YNiC₂ and then move to the three magnetic compounds in order of their volume DyNiC₂, HoNiC₂, and ErNiC₂. This is because the proposed phase diagram suggested that the CDW transition temperatures of the RNiC₂ family have close relationships with their volumes. In a previous report [16,31], three CDWs having different wave vectors have been reported. This was also observed in our paper: IC CDW with $\mathbf{q}_{1ic}:(0.5, 0.5 + \eta, 0)$; C CDW with $\mathbf{q}_{1c}:(0.5, 0.5, 0)$; C CDW with $\mathbf{q}_{2c}:(0.5, 0.5, 0.5)$. In the following part, these notations will be added to avoid confusion.

A. YNiC₂

Figure 1 shows the temperature dependence of the electrical resistivity of nonmagnetic YNiC₂ and the integrated intensities of the satellite reflections: $\mathbf{q}_{2c}:(-1.5, -0.5, 0.5)$; $\mathbf{q}_{2c}:(1.5, 3.5, 2.5)$; and $\mathbf{q}_{1ic}:(1.5, 3.5 + \eta, 3.0)$. A humplike resistivity anomaly, suggestive of possible CDW formation, is observed from 305 to 275 K. The resistivity increases steeply from 305 to 285 K and then sharply drops to 275 K. Below that, the resistivity behaves like a conventional metal and decreases gently down to low temperatures.

X-ray-diffraction measurements were performed to investigate the possibility of CDW formation at the resistance anomaly. The x-ray studies revealed that two kinds of CDWs \mathbf{q}_{1ic} and \mathbf{q}_{2c} compete in the narrow temperature range. Figure 2 shows the oscillation photographs of YNiC₂ based on their 2θ value and indices of main Bragg spots neighboring them. At 280 K, clear satellite reflections $\mathbf{q}_{1ic}:(1.5, 3.5 + \eta, 3.0)$ and $\mathbf{q}_{1ic}:(1.5, 3.5 + \eta, 2.0)$ are observed. The faint traces of these satellite reflections have already been observed

TABLE I. Lattice constants, unit-cell volume, magnetic properties, wave vector, and transition temperature of CDW for $R\text{NiC}_2$ (R : Y, Sm, Gd, Tb, Dy, Ho, and Er) having the CeNiC_2 -type crystal structure with an orthorhombic lattice and $Amm2$ space group. The compounds are sorted by atomic number.

	Lattice parameter [1,35]				Magnetic Property	CDW Property
	$a(\text{\AA})$	$b(\text{\AA})$	$c(\text{\AA})$	$V(\text{\AA}^3)$		
YNiC ₂	3.5715(9)	4.507(1)	6.034(1)	97.13	Nonmagnetic [2]	$\mathbf{q}_{2c}:(0.5, 0.5, 0.5); \lesssim 280$ K $\mathbf{q}_{1ic}:(0.5, 0.5 + \eta, 0); 260\text{--}300$ K Present paper
	3.589	4.505	6.036	97.6		
	3.562(2)	4.509(1)	6.039(2)	97.0		
SmNiC ₂	3.7051(7)	4.5256(7)	6.096(1)	102.22	$T_c = 17.5$ K Ferromagnetic [3]	$\mathbf{q}_{1ic}:(0.5, 0.5 + \eta, 0); 17.5\text{--}148$ K [16]
	3.711(2)	4.524(1)	6.107(4)	102.5		
GdNiC ₂	3.6492(6)	4.5178(5)	6.0726(7)	100.12	$T_N = 22.3$ K Noncollinear, commensurate [7,8]	$\mathbf{q}_{1c}:(0.5, 0.5, 0); \lesssim 83$ K[31] $\mathbf{q}_{1ic}:(0.5, 0.5 + \eta, 0); \sim 83\text{--}205$ K
	3.651(2)	4.518(1)	6.077(3)	100.2		
TbNiC ₂	3.6019(6)	4.5133(6)	6.0570(9)	98.47	$T_N = 25$ K Noncollinear, commensurate [9–11]	$\mathbf{q}_{1c}:(0.5, 0.5, 0); \lesssim 160$ K [31] $\mathbf{q}_{1ic}:(0.5, 0.5 + \eta, 0); \sim 160\text{--}243$ K $\mathbf{q}_{2c}:(0.5, 0.5, 0.5); 25\text{--}128$ K
	3.608(2)	4.514(1)	6.056(3)	98.6		
DyNiC ₂	3.5707(6)	4.5075(6)	6.0410(9)	97.23	$T_N = 7.6$ K Noncollinear [12,14] < 3.3K:C 3.3–5 K:mixture of C and IC 5–7.6 K:IC	$\mathbf{q}_{1c}:(0.5, 0.5, 0);$ < 60K(cooling)/ < 70K(heating) $\mathbf{q}_{2c}:(0.5, 0.5, 0.5); \lesssim 225$ K $\mathbf{q}_{1ic}:(0.5, 0.5 + \eta, 0); \lesssim 180\text{--}275$ K Present paper
	3.561(1)	4.509(1)	6.040(2)	97.0		
HoNiC ₂	3.5469(5)	4.5008(7)	6.0273(9)	96.22	$T_N = 4.0$ K Noncollinear [6,12] < 2.9 K:commensurate 2.9–4.0 K:incommensurate and sinusoidal moment modulation	$\mathbf{q}_{2c}:(0.5, 0.5, 0.5); < 305$ K Present paper
	3.549(2)	4.507(1)	6.033(3)	96.5		
ErNiC ₂	3.5171(7)	4.4924(9)	6.015(1)	95.04	$T_N = 8.5$ K Collinear, commensurate [5,6]	$\mathbf{q}_{2c}:(0.5, 0.5, 0.5); < 345$ K Present paper
	3.518(1)	4.495(1)	6.021(3)	95.2		

at 300 K, which is just below the temperature where the electrical resistivity begins to increase. Subsequently, new clear satellite reflections $\mathbf{q}_{2c}:(1.5, 3.5, 2.5)$ and $\mathbf{q}_{2c}:(1.5, 3.5, 3.5)$ begin to appear at 280 K. Both satellite reflections coexist down to 265 K. Below that temperature, the intensities of

the \mathbf{q}_{2c} satellite reflections increase whereas those of the \mathbf{q}_{1ic} satellite reflections decrease and vanish by 250 K.

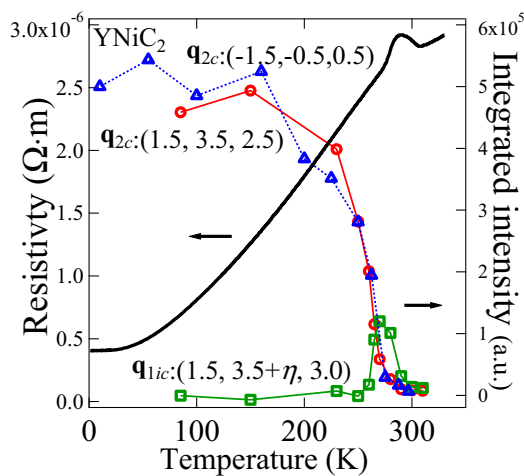


FIG. 1. Temperature dependence of the resistivity and the integrated intensity of satellite reflections of YNiC_2 : $\mathbf{q}_{1ic}:(1.5, 3.5 + \eta, 3.0)$, $\mathbf{q}_{2c}:(1.5, 3.5, 2.5)$, and $\mathbf{q}_{2c}:(-1.5, -0.5, 0.5)$. The intensities of $\mathbf{q}_{1ic}:(1.5, 3.5 + \eta, 3.0)$ and $\mathbf{q}_{2c}:(1.5, 3.5, 2.5)$ were obtained using a commercial x-ray-diffraction measurement system whereas that of $\mathbf{q}_{2c}:(-1.5, -0.5, 0.5)$ was collected employing a four-axis diffractometer. See also Figs. 2 and 3, respectively.

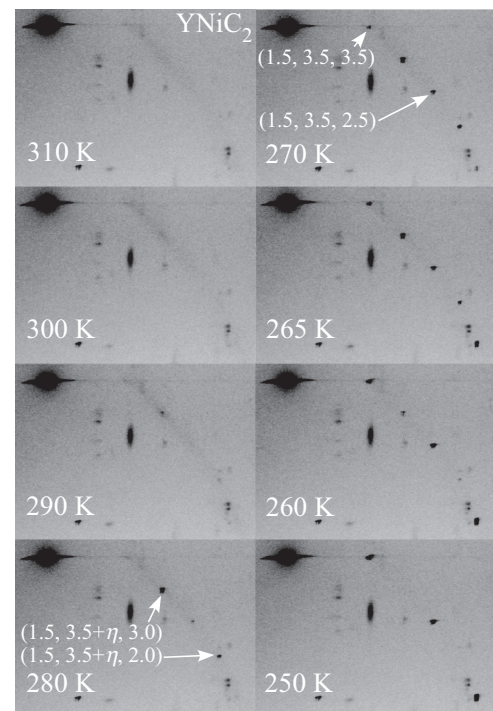


FIG. 2. Oscillation photographs of YNiC_2 near the resistance anomaly from 310 to 250 K. Arrows indicate satellite reflections.

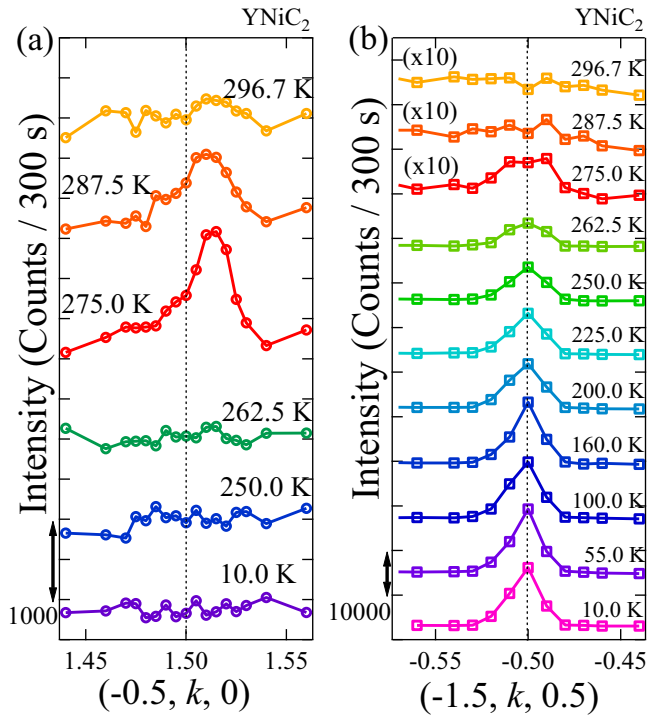


FIG. 3. Temperature dependence of the diffuse scattering profiles of YNiC_2 measured along the \mathbf{b}^* axis at several temperatures: (a) $\mathbf{q}_{1ic}:(-0.5, 1.5 + \eta, 0)$ and (b) $\mathbf{q}_{2c}:(-1.5, -0.5, 0.5)$.

In order to obtain the precise wave vectors of these observed satellite reflections, the scattering profiles were measured. Figures 3(a) and 3(b) show the profiles of $\mathbf{q}_{1ic}:(-0.5, 1.5 + \eta, 0)$ and $\mathbf{q}_{2c}:(-1.5, -0.5, 0.5)$, respectively. The precise wave vector of \mathbf{q}_{1ic} is $(0.5, 0.513 \pm 0.002, 0)$, and that of \mathbf{q}_{2c} is confirmed to be commensurate $(0.5, 0.5, 0.5)$. Based on the oscillation photographs and the scattering profiles, the temperature dependence of the integrated intensities of the satellite reflections are displayed in Fig. 1. In the humplike anomaly, the resistivity increases down to the temperature where the \mathbf{q}_{2c} satellite reflections start to appear and rapidly decreases down to the temperature where the intensity of the \mathbf{q}_{1ic} satellite reflection starts to decrease.

These results indicate that: (I) the appearance of \mathbf{q}_{1ic} and \mathbf{q}_{2c} satellite reflections have close relationships with the humplike resistance anomaly, suggesting the formation of \mathbf{q}_{1ic} CDW and \mathbf{q}_{2c} CDW; (II) in YNiC_2 , these CDWs compete strongly in the narrow temperature range near 270 K, and the stability of the \mathbf{q}_{2c} CDW is superior to that of the \mathbf{q}_{1ic} CDW below that temperature.

B. DyNiC_2

Figure 4 shows the temperature dependence of the electrical resistivity of DyNiC_2 and the integrated intensities of the three kinds of satellite reflections: $\mathbf{q}_{1ic}:(0.5, 1.5 + \eta, 0)$, $\mathbf{q}_{1c}:(0.5, 1.5, 0)$, and $\mathbf{q}_{2c}:(-1.5, -0.5, 0.5)$. The temperature dependence of the resistivity has two remarkable anomalies: A humplike anomaly in the 275–180 K temperature range and a sharp increase below 60 K. A small dent is also observed near 225 K. The lower-temperature anomaly

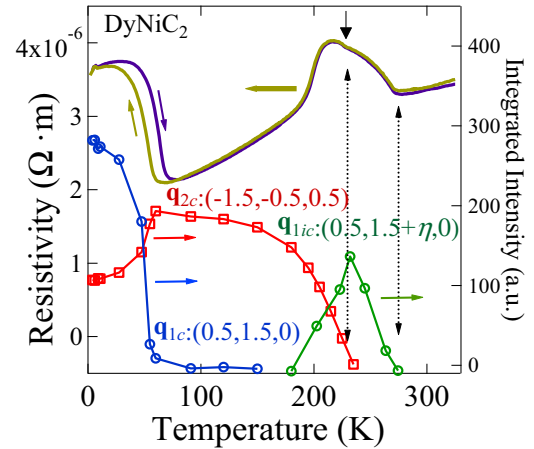


FIG. 4. Temperature dependence of the resistivity and the integrated intensity of satellite reflections for DyNiC_2 : $\mathbf{q}_{1ic}:(0.5, 1.5 + \eta, 0)$, $\mathbf{q}_{1c}:(0.5, 1.5, 0)$, and $\mathbf{q}_{2c}:(-1.5, -0.5, 0.5)$. A black downward arrow indicates a dent in the temperature dependence of the resistivity. (See the text.) The intensities were collected employing a four-axis diffractometer. See also Fig. 5.

has clear hysteresis between decreasing and increasing temperatures.

X-ray-diffraction measurements were performed to investigate the possibility of CDW formation at each resistance anomaly. The x-ray studies revealed that the two kinds of CDWs, \mathbf{q}_{1ic} CDW and \mathbf{q}_{2c} CDW, compete in the humplike resistance anomaly. Figure 5 shows the scattering profiles of the satellite reflections near $(0.5, 1.5, 0)$ and $(-1.5, -0.5, 0.5)$. Near 270 K, where the resistivity starts to increase in the higher-temperature anomaly, the incommensurate satellite reflection $\mathbf{q}_{1ic}:(0.5, 1.5 + \eta, 0)$ appears first. Subsequently, the commensurate satellite reflection $\mathbf{q}_{2c}:(-1.5, -0.5, 0.5)$ appears near 225 K. The appearance of this \mathbf{q}_{2c} satellite reflections is detected as a small dent in the temperature dependence of the resistivity as pointed out above. Below that temperature, the intensity of $\mathbf{q}_{2c}:(-1.5, -0.5, 0.5)$ increases whereas that of $\mathbf{q}_{1ic}:(0.5, 1.5 + \eta, 0)$ decreases rapidly and vanishes by 180 K. Below 60 K, where the lower-temperature anomaly appears, the commensurate satellite reflection $\mathbf{q}_{1c}:(0.5, 1.5, 0)$ appears suddenly and grows. Simultaneously, the intensity of $\mathbf{q}_{2c}:(-1.5, -0.5, 0.5)$ starts to decrease but remains meaningful even at the lowest temperature measured. The temperature dependence of the integrated intensity of $\mathbf{q}_{1ic}:(0.5, 1.5 + \eta, 0)$, $\mathbf{q}_{1c}:(0.5, 1.5, 0)$, and $\mathbf{q}_{2c}:(-1.5, -0.5, 0.5)$, based on the scattering profiles, are shown in Fig. 4. These results indicate that both resistance anomalies, the humplike anomaly from 275 to 180 K and the sharp increase below 60 K, should be interpreted as the formation of IC CDW and C CDW.

In the top part of Fig. 5(a), the peak position of \mathbf{q}_{1ic} moves strangely from $k = 1.49 \pm 0.02$ to 1.504 ± 0.02 , which occurs simultaneously with the appearance of $\mathbf{q}_{2c}:(-1.5, -0.5, 0.5)$ around 225 K. This peak position shift clearly indicates that \mathbf{q}_{1ic} CDW and \mathbf{q}_{2c} CDW coexist intrinsically in the same lattice, not like a phase separation. This peculiar peak shift is likely caused by the rearrangement of constituent atoms to allow the \mathbf{q}_{1ic} and \mathbf{q}_{2c} CDWs to coexist.

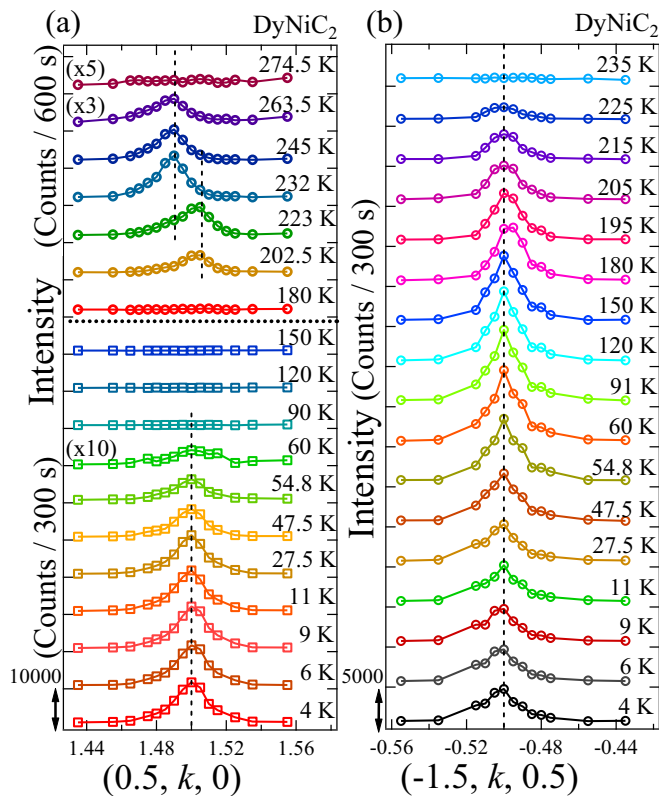


FIG. 5. Temperature dependence of the diffuse scattering profiles of the satellite reflections for DyNi₂ measured along the **b*** axis at several temperatures: (a) (0.5,1.5,0) and (b) (-1.5, -0.5, 0.5). In (a), the measurement of (0.5,1.5,0) was performed in 600 s of the integrated time above 180 K and 300 s below 180 K.

X-ray-diffraction measurements were also performed from 15 to 4 K to investigate the relationships between magnetic ordering and CDWs. Figure 6 shows the temperature dependence of the resistivity and the intensities of the satellite reflections $\mathbf{q}_{1c}:(0.5, 1.5, 0)$ and $\mathbf{q}_{2c}:(-1.5, -0.5, 0.5)$ below 15 K. The intensities of both satellite reflections remain nearly constant, despite the resistance anomalies induced by the formation of magnetic orders, indicating that the interplay between CDWs and magnetic ordering seems to be weak in DyNi₂.

C. HoNi₂

Figure 7 shows the temperature dependence of the electrical resistivity of HoNi₂ and the integrated intensities of the satellite reflection $\mathbf{q}_{2c}:(-1.5, 2.5, 2.5)$. A humplike resistance anomaly, suggestive of the formation of CDW, is observed near 295 K. The resistivity starts to increase sharply at 305 K and reaches a maximum near 287 K. Below that temperature, it gently decreases down to 10 K. In the low-temperature region below 8 K, the resistivity decreases somewhat steeply and increases rapidly at 2.9 K as shown in the upper inset.

Previous studies reported that an incommensurate antiferromagnetic transition occurs at 4.0 K and a magnetic IC-C transition occurs at 2.9 K [12], indicating that the observed resistance anomaly is caused by the magnetic IC-C transition.

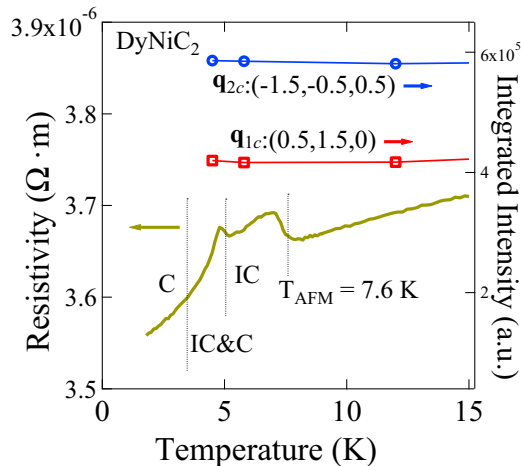


FIG. 6. Low-temperature region of the resistivity for DyNi₂ and the integrated intensity of the satellite reflections around the magnetic transition temperatures: $\mathbf{q}_{1c}:(0.5, 1.5, 0)$ and $\mathbf{q}_{2c}:(-1.5, -0.5, 0.5)$. The intensities were collected employing a four-axis diffractometer. See also Fig. 5. IC and C indicate incommensurate magnetic structure and commensurate magnetic structure, respectively.

No anomaly has been observed in our measurements at the incommensurate antiferromagnetic transition temperature 4.0 K. Similar experimental results were reported in the measurement of the magnetic property [6]. They reported that, in the temperature dependence of the magnetic susceptibility, a clear cusp was observed at 2.9 K and no anomaly was observed at 4.0 K and suggested that such behavior should be ascribed to a sinusoidal magnetic moment modulation in the IC phase.

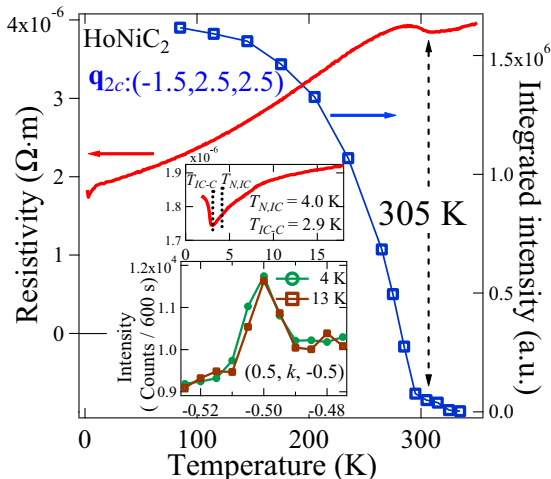


FIG. 7. Temperature dependence of the resistivity and the integrated intensity of the satellite reflection $\mathbf{q}_{2c}:(-1.5, 2.5, 2.5)$ of HoNi₂. The upper inset shows the low-temperature region of the resistivity near the magnetic transition 2.9 K and magnetic IC-C transition temperature 4.0 K. The lower inset shows the diffuse scattering profiles of $\mathbf{q}_{2c}:(0.5, -0.5, -0.5)$ measured along the **b*** axis at 4 and 13 K. Each temperature is below and above 8 K where the resistivity starts to decrease steeply.

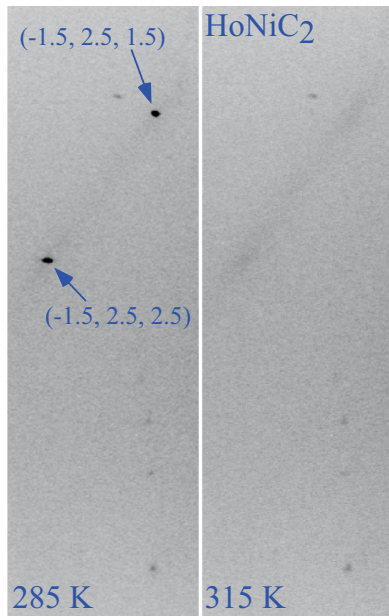


FIG. 8. Oscillation photographs of HoNiC_2 at 285 and 315 K. Each temperature is below and above the resistance anomaly at 295 K. Arrows indicate satellite reflections.

X-ray-diffraction measurements were performed to investigate the possibility of CDW formation. Figure 8 shows the oscillation photographs of HoNiC_2 at 285 and 315 K. Diffuse streaks at 315 K condense into commensurate satellite

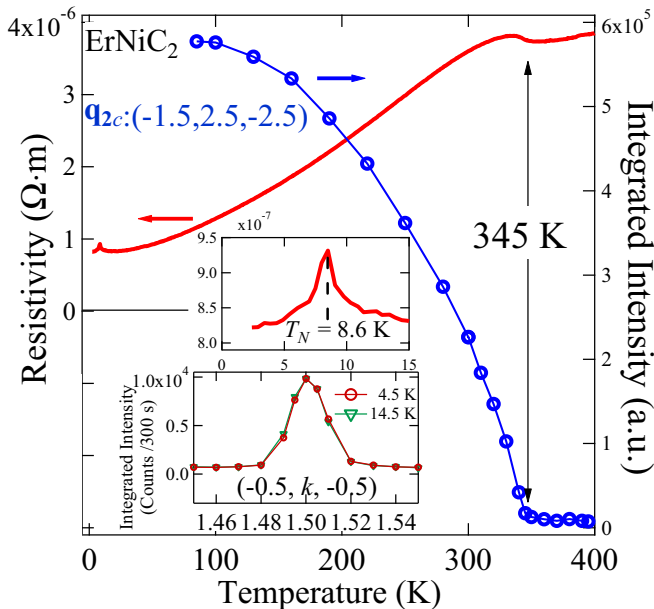


FIG. 9. Temperature dependence of the resistivity and the integrated intensity of the satellite reflection $\mathbf{q}_{2c}:(-1.5, 2.5, -2.5)$ of ErNiC_2 . The upper inset shows the low-temperature region of the resistivity, and the lower inset shows the diffuse scattering profiles of $\mathbf{q}_{2c}:(-0.5, 1.5, -0.5)$ measured along the \mathbf{b}^* axis at 4.5 and 14.5 K. Each temperature is below and above the magnetic transition temperature.

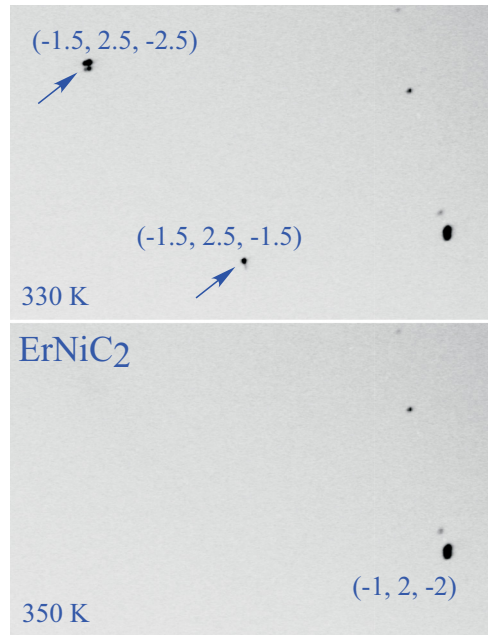


FIG. 10. Oscillation photographs of ErNiC_2 at 330 and 350 K. Each temperature is below and above the resistivity anomaly at 345 K. Arrows indicate satellite reflections.

reflections $\mathbf{q}_{2c}:(-1.5, 2.5, 1.5)$ and $(-1.5, 2.5, 2.5)$ at 285 K. Based on the intensities of the oscillation photographs, the temperature dependence of the integrated intensity of $\mathbf{q}_{2c}:(-1.5, 2.5, 2.5)$ is displayed in Fig. 7. These results indicate that the appearance of \mathbf{q}_{2c} satellite reflections have close relationships with the humplike anomaly, indicating the formation of \mathbf{q}_{2c} CDW.

Scattering profiles of the satellite reflections were measured in the 13 to 4 K to investigate the relationships between the resistance decrease below 8 K and \mathbf{q}_{2c} CDW. The lower inset of Fig. 7 shows the scattering profiles of the satellite reflections $\mathbf{q}_{2c}:(0.5, -0.5, -0.5)$. The intensity is relatively constant in this temperature range. Although it is unclear why the resistivity decreases rapidly below 8 K, one possible explanation could be a decrease in the antiferromagnetic fluctuation toward the ordering temperature. A similar decrease in the resistivity was seen in PrNiC_2 having no magnetic transition down to 1.5 K [22].

D. ErNiC_2

Figure 9 shows the temperature dependence of the electrical resistivity of ErNiC_2 and the integrated intensities of the satellite reflection $\mathbf{q}_{2c}:(-1.5, 2.5, -2.5)$. In this compound, a humplike resistance anomaly suggestive of CDW formation is observed near 330 K. The resistivity starts to increase at 345 K and reaches a maximum near 330 K. Below that temperature, the resistivity decreases gently. In the low-temperature region below 15 K, the temperature dependence of the electrical resistivity has a peak structure at the antiferromagnetic ordering temperature 8.6 K as shown in the upper inset.

X-ray-diffraction measurements were performed to confirm C CDW formation. Figure 10 shows the oscillation photographs for ErNiC_2 at 330 and 350 K. The satellite reflections

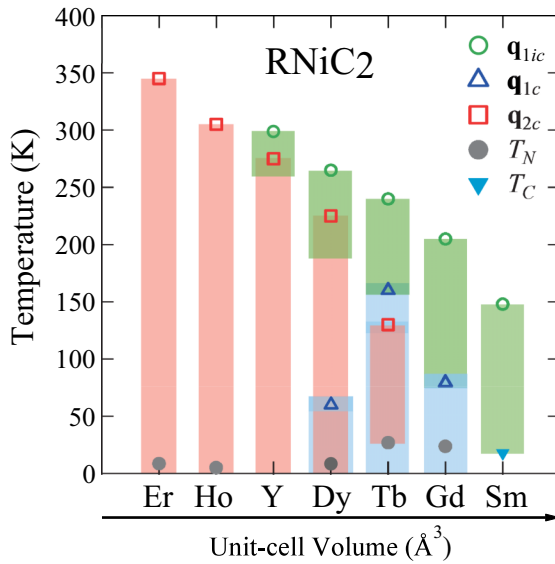


FIG. 11. Phase diagram of the CDW transition temperatures for $RNiC_2$ (R : Er, Ho, Y, Dy, Tb, Gd, and Sm). Transitions of q_{1ic} , q_{1c} , and q_{2c} CDWs, the antiferromagnetic transition T_N , and the ferromagnetic transition T_C are plotted. The data for $SmNiC_2$, $GdNiC_2$, and $TbNiC_2$ were obtained from Refs. [16,31]. Temperature ranges where each satellite reflection is observed are indicated by vertical thick bars and hystereses observed in transport measurements are shown by thick horizontal bars.

are indexed based on their 2θ value and indices of main Bragg spots neighboring them. In this compound, diffuse streaks, the intensity of which was 10^{-2} as high as that of main Bragg peaks around the satellite reflections, have not been observed. This point is clearly different from the CDW transition of $HoNiC_2$. The temperature dependence of the integrated intensity of $q_{2c}:(-1.5, 2.5, -2.5)$ based on the results of the oscillation photographs is displayed in Fig. 9. These results indicate that the appearance of q_{2c} satellite reflections have close relationships with the hump-like anomaly, indicating the formation of C CDW.

The scattering profiles of satellite reflections were measured in the temperature region from 14.5 to 4.5 K to investigate the relationships between the magnetic ordering at 8.6 K and the q_{2c} CDW. The lower inset of Fig. 9 shows the scattering profiles of the satellite reflections $q_{2c}:(-0.5, 1.5, -0.5)$. The intensity is near constant in this temperature range, indicating that the interplay between CDW and magnetic ordering seems to be weak in $ErNiC_2$, such as in the case of $DyNiC_2$.

IV. DISCUSSION

We first discuss the CDW transitions of $RNiC_2$. Figure 11 shows the CDW phase diagram for $RNiC_2$ (R : Er, Ho, Y, Dy, Tb, Gd, and Sm). This phase diagram is relevant as an extension of that proposed by Shimomura *et al.* [31]. Although the unit-cell volume of $YNiC_2$ is almost the same as that of $DyNiC_2$ as shown in Table I, we place $YNiC_2$ between $HoNiC_2$ and $DyNiC_2$ in this phase diagram. It is because $YNiC_2$ has two kinds of CDWs, q_{1ic} CDW in the narrow temperature range from 260 to 290 K and q_{2c} CDW, which

suppresses q_{1ic} CDW, whereas $HoNiC_2$ has only one CDW, q_{2c} CDW, and $DyNiC_2$ has three kinds of CDWs, q_{1ic} CDW, q_{1c} CDW, and q_{2c} CDW. The results of $SmNiC_2$, $GdNiC_2$, and $TbNiC_2$ are also shown for discussion [16,31].

This phase diagram features interrelationships among the three kinds of CDWs, q_{1ic} CDW, q_{1c} CDW, and q_{2c} CDW. This point clearly differs from that proposed by Roman *et al.* [32] and Kolincio *et al.* [33], which contained only the two CDWs q_{1ic} CDW and its IC-C transition (q_{1ic} CDW). Only the q_{1ic} CDW exists in $SmNiC_2$ and the q_{1ic} CDW and the q_{1c} CDW resulted from the IC-C transition exist in $GdNiC_2$ [16,31]. An IC-C transition is generally caused by the commensurability effect and has been observed in several CDW materials with wave vectors being nearly commensurate with the underlying lattice, such as *orthorhombic* TaS_3 and the quasi-one-dimensional organic conductor TTF-TCNQ (tetrathiafulvalene-tetracyanoquinodimethane) [36–41]. The IC-C transition in $GdNiC_2$ is likely of this same type. In $TbNiC_2$, the q_{2c} CDW appears to be coexisting with q_{1c} CDW, replaced by q_{1ic} CDW through the IC-C transition [31]. In this material, the stability of q_{1c} CDW is superior to that of q_{2c} CDW because the CDW transition temperature of q_{1c} CDW is higher than that of q_{2c} CDW, and the q_{2c} CDW with long-range order was first discovered in $TbNiC_2$ and only diffuse spots without long-range order have been observed in $RNiC_2$ composed of earlier lanthanide atoms $SmNiC_2$ and $GdNiC_2$ [16,31]. This might partially be supported by the fact that only the q_{2c} CDW is suppressed at the antiferromagnetic temperature in $TbNiC_2$. In $DyNiC_2$, the q_{2c} CDW stabilizes more than that in $TbNiC_2$ because the transition temperature of q_{2c} CDW in $DyNiC_2$ is about 100 K higher than that in $TbNiC_2$. The results of $DyNiC_2$ indicate that the stability of the q_{2c} CDW is superior to that of the q_{1ic} CDW and almost equal to that of the q_{1c} CDW in this material. This is because the appearance of the q_{2c} CDW rapidly suppresses the q_{1ic} CDW, and the q_{1c} CDW appears in the low-temperature region below 60 K, despite the existence of the q_{2c} CDW. In $YNiC_2$, the stability of the q_{2c} CDW must be superior to those of the q_{1ic} and q_{1c} CDWs, and this explains why the q_{1c} CDW does not appear in this material. In $HoNiC_2$ and $ErNiC_2$ in which the q_{1ic} and q_{1c} CDWs do not appear, the stability of the q_{2c} CDW is much superior to those of the other two CDWs. The competition among q_{1ic} , q_{1c} , and q_{2c} CDWs provides the rich and complicated CDW phase diagram of the $RNiC_2$ family.

We arrive at an important question regarding the formation mechanism of the q_{1c} CDW below 60 K in $DyNiC_2$. The q_{1c} CDW does not appear through an IC-C transition but appears independently in the presence of the q_{2c} CDW. A similar problem also exists in $TbNiC_2$ in which the q_{2c} CDW appears in the presence of the q_{1ic} CDW. An electronic structure with one CDW cannot be suitable for the Fermi-surface nesting that causes another CDW, indicating that we cannot simply adopt a general nesting scenario for a CDW formation for this case and need to cope with coexistence of multiple CDWs in a material. A crystal structure analysis in the presence of multiple CDWs or a detailed structural analysis of precursory phenomena of the secondary CDW transition will be needed.

Presently, why the q_{2c} CDW stabilizes more than the q_{1c} and q_{1ic} CDWs with decreasing the unit-cell volume

remains an unanswered question. In the $R\text{NiC}_2$ family, the lanthanides contraction decreases the unit-cell volumes with increasing constituent rare-earth atomic number. The comparison between the lattice parameters of GdNiC_2 and ErNiC_2 in Table I indicates that the a -axis lattice parameter shrinks the most -3.6% as compared with -0.6% and -0.8% for the b axis and c axis, respectively. Since the a axis is along the relative one-dimensional (1D) anisotropy of the electronic structure, this comparison simply suggests that the 1D nature of the electronic structure is enhanced. A recent first-principles calculation of chemical and hydrostatic pressure effects on $R\text{NiC}_2$ also could not clarify the reason why the \mathbf{q}_{2c} CDW stabilizes more than the \mathbf{q}_{1c} and \mathbf{q}_{1ic} CDWs from the viewpoint of a generalized susceptibility calculated from an obtained electronic structure [42,43].

At this stage, we consider Coulomb interaction in a crystal as one possible answer for this question. A CDW phase is microscopically regarded as a bundle of charge density waves on atomic chains along a certain direction in a crystal, and the Coulomb interaction works three dimensionally among the charge density waves formed on the atomic chains. This Coulomb effect, which is regarded as the interchain coupling effect or three-dimensional effect in a low-dimensional electronic system, generally determines the phase relation among charge density waves on neighboring atomic chains in a crystal and plays an essential role for realizing a CDW phase [18]. This effect will naturally affect which CDW is most stabilized in a real material in which multiple CDWs compete from the viewpoint of a generalized susceptibility in a reciprocal space. The crystal structure analysis of SmNiC_2 with \mathbf{q}_{1ic} CDW clarified that, although the CDW should be considered to be commensurate from a microscopic viewpoint, frustrated interchain coupling compelled the commensurate CDW to be macroscopically incommensurate [21]. If this understanding applies to the whole $R\text{NiC}_2$ family, the Coulomb interaction is a promising answer for the question why the \mathbf{q}_{2c} CDW stabilizes more than the \mathbf{q}_{1c} and \mathbf{q}_{1ic} CDWs in $R\text{NiC}_2$ materials having smaller volumes. It is because decreasing unit-cell volumes makes interchain distances decrease and the importance of the interchain coupling effect increase, which compels a phase shift of π between neighboring microscopic charge density waves to be fixed and makes a commensurate CDW phase more stable. A crystal structure analysis of a $R\text{NiC}_2$ compound with \mathbf{q}_{2c} CDW will be needed to solve this important question.

This consideration could explain why diffuse streaks are not observed in ErNiC_2 but in HoNiC_2 . The \mathbf{q}_{2c} CDW in ErNiC_2 stabilizes much more than that in HoNiC_2 because the transition temperature of the \mathbf{q}_{2c} CDW in ErNiC_2 is about 40 K higher than that in HoNiC_2 . Judging from the phase diagram in Fig. 11, the higher stability of the \mathbf{q}_{2c} CDW is clearly due to the lattice volume effect, and the smaller lattice volume will lead to stronger Coulomb interaction, which three dimensionally works among microscopic charge density waves in a crystal as mentioned above. This three-dimensional effect can be expected to make diffuse streaks

as the precursor of a phase transition in a low-dimensional electronic system appear in a quite narrow temperature range just above its transition temperature or change into diffuse spots [18].

Lastly, we mention the possible existence of interplay between CDW and magnetism in DyNiC_2 , HoNiC_2 , and ErNiC_2 . The experimental results of DyNiC_2 and ErNiC_2 suggest no clear interplay between CDWs and magnetic orderings in these materials. In the previous studies of SmNiC_2 and TbNiC_2 [16,31], a rapid resistance decrease just below a magnetic transition was observed, which means the destruction of CDW and the existence of the interplay between CDWs and magnetic orderings. Such resistance decreases were not observed in the temperature dependence of the resistivity for DyNiC_2 and ErNiC_2 during our experiments, indicating that the interplay between CDWs and magnetism was weak in them. Concerning HoNiC_2 , the resistivity measurement should first be performed at a temperature sufficiently lower than the commensurate magnetic ordering temperature 2.9 K and investigate whether a rapid decrease in the resistance occurs or not. This experiment is important from the viewpoint whether the difference in the commensurate antiferromagnetic order, collinear (ErNiC_2), or noncollinear (HoNiC_2) affects interplay between CDWs and magnetism in $R\text{NiC}_2$ or not and will be an urgent future work.

V. CONCLUSIONS

We performed single-crystal x-ray-diffraction experiments and electrical resistivity measurements of $R\text{NiC}_2$ (R : Y, Dy, Ho, and Er). At the temperatures where their resistivities showed anomalies, we found structural changes accompanied by the appearance of any one of three kinds of satellite reflections having different wave vectors, incommensurate $\mathbf{q}_{1ic}:(0.5, 0.5 + \eta, 0)$ and commensurate $\mathbf{q}_{1c}:(0.5, 0.5, 0)$ and $\mathbf{q}_{2c}:(0.5, 0.5, 0.5)$. We interpreted these resistance anomalies as the formation of CDWs. We found strong competition between the \mathbf{q}_{1ic} CDW and the \mathbf{q}_{2c} CDW in DyNiC_2 and YNiC_2 and that only the \mathbf{q}_{2c} CDW existed in HoNiC_2 and ErNiC_2 . Based on the experimental results, including those of SmNiC_2 , GdNiC_2 , and TbNiC_2 , we discussed the CDW transitions of the $R\text{NiC}_2$ family. We also found that the interplay between CDWs and magnetism was weak in DyNiC_2 and ErNiC_2 .

ACKNOWLEDGMENTS

The authors thank Prof. N. Hanasaki (Osaka University) and Prof. S. Shimomura (Kyoto Sangyo University) for valuable discussions and S. Okabe (Okayama University) for experimental support. This work was partly supported by a Grant-in-Aid for Scientific Research (C) (Grant No. 24540374) and (C) (Grant No. 26400362) from the Ministry of Education, Culture, Sports, Science and Technology, Japan (MEXT).

[1] W. Jeitschko and M. H. Gerss, *J. Less. Common. Met.* **116**, 147 (1986).

[2] P. Kotsanidis, J. Yakinthos, and E. Gamari-Seale, *J. Less Common Met.* **152**, 287 (1989).

- [3] H. Onodera, Y. Koshikawa, M. Kosaka, M. Ohashi, H. Yamauchi, and Y. Yamaguchi, *J. Magn. Magn. Mater.* **182**, 161 (1998).
- [4] J. K. Yakinthos, P. A. Kotsanidis, W. Schäfer, and G. Will, *J. Magn. Magn. Mater.* **89**, 299 (1990).
- [5] J. K. Yakinthos, P. A. Kotsanidis, W. Schäfer, and G. Will, *J. Magn. Magn. Mater.* **102**, 71 (1991).
- [6] Y. Koshikawa, H. Onodera, M. Kosaka, H. Yamachi, M. Ohashi, and Y. Yamaguchi, *J. Magn. Magn. Mater.* **173**, 72 (1997).
- [7] S. Matsuo, H. Onodera, M. Kosaka, H. Kobayashi, M. Ohashi, H. Yamauchi, and Y. Yamaguchi, *J. Magn. Magn. Mater.* **161**, 255 (1996).
- [8] H. Onodera, H. Amanai, S. Matsuo, M. Kosaka, H. Kobayashi, M. Ohashi, and Y. Yamaguchi, *Sci. Rep. RITU A* **45**, 1 (1997).
- [9] J. K. Yakinthos, P. A. Kotsanidis, W. Schäfer, and G. Will, *J. Magn. Magn. Mater.* **81**, 163 (1989).
- [10] H. Onodera, N. Uchida, M. Ohashi, H. Yamauchi, Y. Yamaguchi, and N. Sato, *J. Magn. Magn. Mater.* **137**, 35 (1994).
- [11] N. Uchida, H. Onodera, M. Ohashi, Y. Yamaguchi, N. Sato, and S. Funahashi, *J. Magn. Magn. Mater.* **145**, L16 (1995).
- [12] J. K. Yakinthos, P. A. Kotsanidis, W. Schäfer, and G. Will, *J. Magn. Magn. Mater.* **136**, 327 (1994).
- [13] K. Motoya, K. Nakaguchi, N. Kayama, K. Inari, J. Akimitsu, K. Izawa, and T. Fujita, *J. Phys. Soc. Jpn.* **66**, 1124 (1997).
- [14] H. Onodera, M. Ohashi, H. Amanai, S. Matsuo, H. Yamauchi, Y. Yamaguchi, S. Funahashi, and Y. Morii, *J. Magn. Magn. Mater.* **149**, 287 (1995).
- [15] H. Michor, S. Steiner, A. Schumer, M. Hembara, V. Levitsky, V. Babizhetskyy, and B. Kotur, *J. Magn. Magn. Mater.* **441**, 69 (2017).
- [16] S. Shimomura, C. Hayashi, G. Asaka, N. Wakabayashi, M. Mizumaki, and H. Onodera, *Phys. Rev. Lett.* **102**, 076404 (2009).
- [17] M. Murase, A. Tobo, H. Onodera, Y. Hirano, T. Hosaka, S. Shimomura, and N. Wakabayashi, *J. Phys. Soc. Jpn.* **73**, 2790 (2004).
- [18] G. Grüner, *Density Waves in Solids* (Perseus, Cambridge, UK, 2000).
- [19] J. Laverock, T. D. Haynes, C. Uffeld, and S. B. Dugdale, *Phys. Rev. B* **80**, 125111 (2009).
- [20] S. Steiner, H. Michor, O. Sologub, B. Hinterleitner, F. Höfenstock, M. Waas, E. Bauer, B. Stöger, V. Babizhetskyy, V. Levitsky, and B. Kotur, *Phys. Rev. B* **97**, 205115 (2018).
- [21] A. Wölfel, L. Li, S. Shimomura, H. Onodera, and S. van Smaalen, *Phys. Rev. B* **82**, 054120 (2010).
- [22] N. Yamamoto, R. Kondo, H. Maeda, and Y. Nogami, *J. Phys. Soc. Jpn.* **82**, 123701 (2013).
- [23] K. K. Kolincio, K. Gornicka, M. J. Winiarski, J. Strychalska-Nowak, and T. Klimczuk, *Phys. Rev. B* **94**, 195149 (2016).
- [24] N. Hanasaki, S. Shimomura, K. Mikami and Y. Nogami, H. Nakao, and H. Onodera, *Phys. Rev. B* **95**, 085103 (2017).
- [25] K. K. Kolincio, M. Roman, M. J. Winiarski, J. Strychalska-Nowak, and T. Klimczuk, *Phys. Rev. B* **95**, 235156 (2017).
- [26] N. Hanasaki, Y. Nogami and M. Kakinuma, S. Shimomura, M. Kosaka, and H. Onodera, *Phys. Rev. B* **85**, 092402 (2012).
- [27] H. Lei, K. Wang, and C. Petrovic, *J. Phys.: Condens. Matter* **29**, 075602 (2016).
- [28] F. Galli, S. Ramakrishnan, T. Taniguchi, G. J. Nieuwenhuys, J. A. Mydosh, S. Geupel, J. Lüdecke, and S. van Smaalen, *Phys. Rev. Lett.* **85**, 158 (2000).
- [29] F. Galli, R. Feyerherm, R. W. A. Hendrikx, E. Dudzik, G. J. Nieuwenhuys, S. Ramakrishnan, S. D. Brown, S. Van Smaalen, and J. A. Mydosh, *J. Phys.: Condens. Matter* **14**, 5067 (2002).
- [30] S. van Smaalen, M. Shaz, L. Palatinus, P. Daniels, F. Galli, G. J. Nieuwenhuys, and J. A. Mydosh, *Phys. Rev. B* **69**, 014103 (2004).
- [31] S. Shimomura, C. Hayashi, N. Hanasaki, K. Ohnuma, Y. Kobayashi, H. Nakao, M. Mizumaki, and H. Onodera, *Phys. Rev. B* **93**, 165108 (2016).
- [32] M. Roman, J. Strychalska-Nowak, T. Klimczuk, and K. K. Kolincio, *Phys. Rev. B* **97**, 041103(R) (2018).
- [33] K. K. Kolincio, M. Roman, and T. Klimczuk, *Phys. Rev. B* **99**, 205127 (2019).
- [34] R. Kondo, S. Kagoshima, and J. Harada, *Rev. Sci. Instrum.* **76**, 093902 (2005).
- [35] K. N. Semenenko, A. A. Putyatin, I. V. Nikol'skaya, and V. V. Burnasheva, *Russ. J. Inorg. Chem.* **28**, 943 (1983).
- [36] W. L. McMillan, *Phys. Rev. B* **14**, 1496 (1976).
- [37] K. Tsutsumi, T. Sambongi, S. Kagoshima, and T. Ishiguro, *J. Phys. Soc. Jpn.* **44**, 1735 (1978).
- [38] C. Roucau, *J. Phys. Colloq. (Paris)* **44**, C3-1725 (1983).
- [39] K. Inagaki, M. Tsubota, K. Higashiyama, K. Ichimura, S. Tanda, K. Yamamoto, N. Hanasaki, N. Ikeda, Y. Nogami, T. Ito, and H. Toyokawa, *J. Phys. Soc. Jpn.* **77**, 093708 (2008).
- [40] P. Bak and V. J. Emery, *Phys. Rev. Lett* **36**, 978 (1976).
- [41] K. Inagaki and S. Tanda, *Phys. Rev. B* **97**, 115432 (2018).
- [42] B. Woo, S. Seo, E. Park, J. H. Kim, D. Jang, T. Park, H. Lee, F. Ronning, J. D. Thompson, V. A. Sidorov, and Y. S. Kwon, *Phys. Rev. B* **87**, 125121 (2013).
- [43] J. N. Kim, C. Lee and J.-H. Shim, *New J. Phys.* **15**, 123018 (2013).